

Towards the hydrologic and bed load monitoring from high-frequency seismic noise in a braided river: The “torrent de St Pierre”, French Alps

Arnaud Burtin^{a,b,*}, Rodolphe Cattin^c, Laurent Bollinger^d, Jérôme Vergne^e, Philippe Steer^c, Alexandra Robert^b, Nathaniel Findling^b, Christel Tiberi^c

^a University of Cambridge, Department of Earth Sciences, Cambridge CB2 3EQ, United Kingdom

^b Laboratoire de Géologie, École Normale Supérieure de Paris, CNRS UMR 8538, Paris, France

^c Université Montpellier 2, CNRS, Géosciences Montpellier, Montpellier, France

^d CEA, DAM, DIF, Arpajon, France

^e École et Observatoire des Sciences de la Terre, CNRS UMR 7516, Strasbourg, France

ARTICLE INFO

Article history:

Received 17 May 2010

Received in revised form 6 June 2011

Accepted 13 July 2011

Available online 23 July 2011

This manuscript was handled by Philippe Baveye, Editor-in-Chief

Keywords:

Braided river
Sediment transport
River seismic noise
Bed load monitoring

SUMMARY

We explore the use of seismic noise produced by rivers to monitor the bed load transport in the case of a low-discharge braided river in the French Alps: the “torrent de St Pierre”. For this purpose, we deployed two dedicated seismic networks during summers 2007 and 2008, for which the characteristics of the recorded continuous signal are similar despite changes in the sensor locations. For dry weather conditions, only melting of nearby glaciers controls the supply of water to the stream. In these conditions, the river hydrology and the seismic energy in the 2–80 Hz frequency band both follow a diurnal fluctuation similar to the thermal amplitude. In contrast during rainfall episodes, the temperature variation fails to explain the hydrodynamic changes. Dense cloud covers reduce glacier melting and the recorded seismic energy denotes bursts of high-frequency seismic noise well correlated with water level data. Comparisons between the recorded seismic signals and the collected hydrological and sediment load data indicate that a frequency band of 3–9 Hz best explains the water level changes and thus the seismic waves coming from the flow turbulence. These analyses also reveal the presence of a seismic noise threshold that might be linked to the water shear stress exerted by the flowing water. Using the seismic energy in this frequency band as a proxy of the fluvial shear stress, the seismic–hydrologic relationship may be sensitive to variations in bed load transport. The spectral content of the seismic energy shows patterns consistent with the mobilization of sediment particles. From the interpretations of the seismic wave attenuation of river sources, we finally propose that stations at a distance from the stream less than 50 m are able to record most sediment particles. Farther stations are still useful during extreme events when largest grain sizes are mobilized. More generally this study demonstrates the feasibility of using the river seismic signal to survey bed load transport in various river types from small braided mountain rivers like the “torrent de St Pierre” to the large entrenched Himalayan rivers.

© 2011 Elsevier B.V. All rights reserved.

1. Introduction

Sediment transport is a key process in the evolution of alluvial channel patterns (e.g., Schumm, 1986; van den Berg, 1995). Over the last decade many works have highlighted the strong influence of bed load transport on bank erosion, slope failure hazards, river profile evolution as well as on long term incision rate (e.g., Sklar and Dietrich, 1998; Tucker and Whipple, 2002; Attal and Lavé, 2006; Turowski et al., 2007; Burtin et al., 2009). River abrasion is a complex process that illustrates numerous feedbacks. For instance river bed load has two antagonist effects: bed load

impacts are efficient tools to damage the river bedrock but a bed load cover on the streambed is a relevant shield to river incision (Sklar and Dietrich, 2001). Thus, in order to predict or even simply to estimate erosion rate, an accurate monitoring of bed load availability is required. Therefore, monitoring bed load transport is a primary challenge for the comprehension of orogenic erosion processes. Continuous and spatially-dense measurements of river bed load are nevertheless difficult or even impossible to assess with the commonly used methods, which include sediment samplers, traps or hydrophones (Eugene, 1951; Leopold and Emmett, 1976; Belleudy et al., 2010). Indeed, while most of the bed load mobilization occurs during extreme floods, high river discharges prevent direct in situ measurements. To overcome this major limitation, some studies assume that the volume of the bed load is lower than 10% of the suspended sediment flux, a parameter much easier to

* Corresponding author. Address: University of Cambridge, Department of Earth Sciences, Cambridge CB2 3EQ, United Kingdom. Tel.: +44 12237 64368.

E-mail address: ab941@cam.ac.uk (A. Burtin).

estimate (e.g., Lane and Borland, 1951). However, studies in the Himalayan Range indicate that this presumed “bed load to suspended load” ratio underestimates the bed load fraction. This latter may be as high as 50% of the total sediment load (Galy and France-Lanord, 2001; Pratt-Sitaula et al., 2007).

The ability to record spatial and temporal variations is required for bed load monitoring, and standard sediment sampling approaches do not meet these conditions. Therefore, in the past years, several studies have discussed the use of remote sensors to achieve such a monitoring (e.g., Bedeus and Ivicsics, 1964; Johnson and Muir, 1969; Thorne, 1986). In most works, acoustic sensors were employed to record the impact of sediment grains on the streambed or steel plates and pipes (e.g., Thorne and Hanes, 2002; Bogen and Moen, 2003; Froehlich, 2003). Some of these methods relate the amplitude of the acoustic signal to an impact when it exceeds a predefined threshold (Rickenmann and McArdell, 2007). This strategy needs a calibration which depends on the site conditions, like flow intensity and sediment properties (Rickenmann and McArdell, 2008). More generally the spatial extent obtained with acoustic sensors is limited. This approach implies therefore the deployment of a very large number of sensors to cover a small catchment.

Another remote sensing approach is offered by the ability for seismic sensors to record ground vibrations produced by sediments impacting the streambed. This technique brings some advantages since there is no need to couple the instruments with steel plates as for hydrophones or piezoelectric sensors. Furthermore in contrast to in situ techniques, the seismic stations are installed outside the stream and are sheltered from the largest floods. Govi et al. (1993) have shown the potential of seismic records to monitor the bed load transport by comparing the average amplitude of the raw signal with hydraulic and sediment observations. However, the amplitude alone does not explore the full content and information of such a monitoring. Thus, we have recently developed an alternative approach in which the bed load transport is studied through the spectral analysis of the high-frequency river seismic noise (Burtin et al., 2008). With an array of seismic sensors, this technique continuously records spatial and temporal variations in bed load movement over a large region (Burtin et al., 2010).

Up to now this seismic/spectral analysis strategy of bed load estimates has only been applied in central Nepal along the Trisuli River, which is a steep slope and entrenched river with a straight to meandering channel pattern and typical water discharges of 500–2000 m³/s (Lavé and Avouac, 2001). Here, using a dedicated passive seismological experiment we extend our approach to braided river patterns with lower water discharges (~1–5 m³/s). During summers 2007 and 2008, we have deployed a seismic array along the “torrent de St Pierre”, a proglacial gravel-bed river in the “Pré de Madame Carle” located in the “Massif des Écrins” (French Alps; Fig. 1). This site has been selected since the river has a regular and high variability in the water discharge and sediment load. Furthermore, the stream has already been studied by a couple of hydrological experiments (Meunier et al., 2006; Stott and Mount, 2007). In summer season, both studies noticed a daily fluctuation of the river hydrology, which is associated with the melting of snow and ice from two upstream glaciers: the “Glacier Blanc” and the “Glacier Noir” (Fig. 1). Thus, during the ablation season and when no rainfall episode occurs, the water supply is mostly correlated to the diurnal fluctuation of temperature.

The purpose of this study is to investigate the potential of seismometers to record bed load motions associated with rapid changes of water discharge in a braided river. Our approach is based on a wide dataset including hydrological, river sediment load and high-frequency seismic noise measurements that have been jointly acquired during summers 2007 and 2008. After a brief description of the deployed seismological network and the

measured hydrological parameters, we proceed to their detailed analyses. Next, we investigate the possible relationship between the seismic noise and the hydrodynamics of the studied river. Finally, we show that the seismic monitoring of river sediment transport, initially developed for a Himalayan entrenched river, could be applied to various alluvial channel patterns with different stream powers and grain size distributions.

2. Experiment descriptions

2.1. Seismic monitoring

During summers 2007 and 2008, we carried out two distinct seismic experiments. For the first one (hereafter named phase 1), we deployed a passive seismological network of eleven stations from July to the early September of 2007 (Julian day 190–247). The second experiment (hereafter named phase 2) consisted of three seismological stations that recorded data during September 2008, from Julian day 245 to 248. For both arrays, the seismic instruments were installed at distances of 15–200 m from the stream and with an overall geometrical aperture of 5 km (Fig. 1). We used intermediate-band seismometers (velocity-meters) Guralp CMG-40T and short-period seismometers SerCEL L22. We employed two types of 24-bit recording systems: the Reftek RT130 and the Nanometrics TAURUS acquisition system. We set the sampling rate to 200 samples per second. This value allows us to monitor seismic signals up to frequencies of 80 Hz, once we take into account the Nyquist frequency and the anti-alias low-pass filter. We buried the seismological sensors in holes of 0.5–1 m depth and the power was supplied by batteries and solar panels (Fig. 1). During phase 1, we settled the seismological stations to assess the seismic noise related to the various features of the “torrent de St Pierre”. We installed the instruments (denoted by BOL##) along the “torrent du Glacier Blanc”, the “torrent du Glacier Noir”, in the braided plain and at the outlet of the “Pré de Madame Carle” where the stream becomes highly turbulent due to an increase of the river gradient. To discriminate high-frequency human seismic noise from natural sources, we installed the station BOL02 in the vicinity of the road that borders the braided plain and which stands for the main source of human activity (Fig. 1). During phase 2, we set all stations (denoted by ECR0#) in the braided plain far from human disturbances along a profile perpendicular to the river. We used this geometry to investigate the attenuation properties of the potential river seismic sources. With these two geometrical settings, we built dedicated seismological arrays to monitor the hydrology of the river and to survey the bed load transport.

2.2. Stream monitoring

Concurrently with the river seismic monitoring, we performed bed load and hydrological measurements (water level and flow velocity), and we used available rainfall and temperature data. During phase 1, we conducted three campaigns of measurements during the three maintenance services of the seismic stations: from the 8th to 10th of July, from the 1st to 2nd of August and on the 2nd of September. During the four days of phase 2, we monitored the hydrology of the stream as often as possible to assess the temporal variations of bed load transport associated with river discharge changes. For both phases, we measured the flow velocity with a propeller current meter OTT along a river section with a vertical and a horizontal sampling rate of 0.1 and 1 m, respectively. At each bottom point of the river section, we performed a bed load estimate with a Helley–Smith sampler with a 0.15 × 0.15 m entrance and 0.25 × 10⁻³ m mesh sample bag (Helley and Smith,

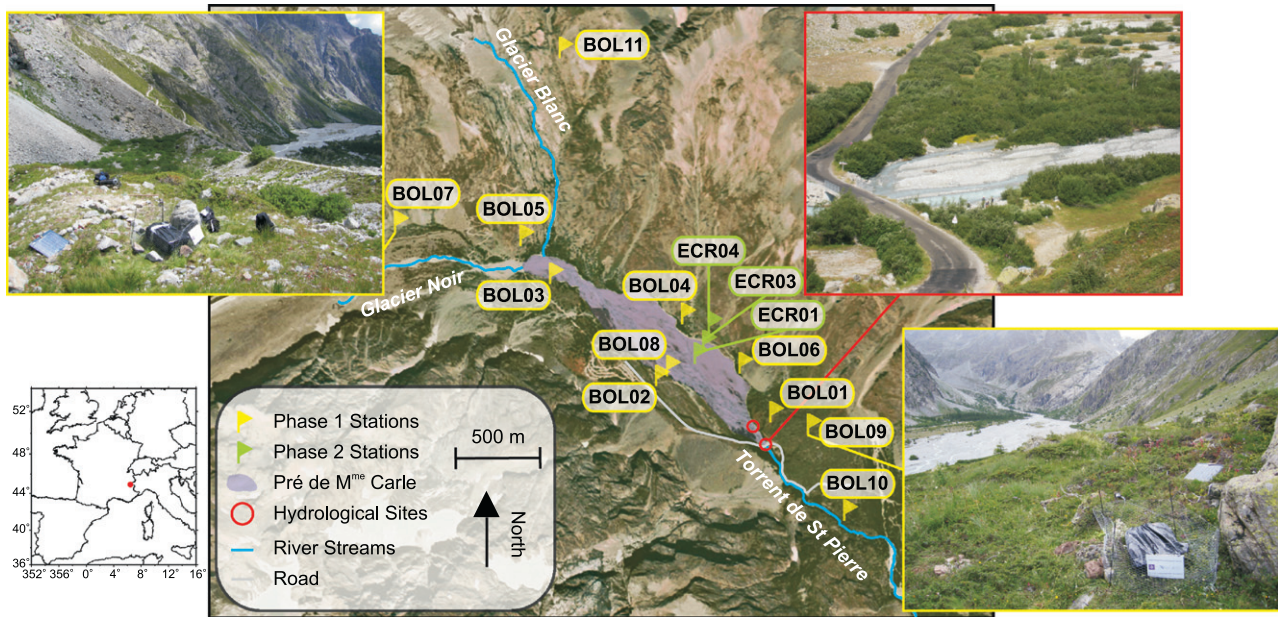


Fig. 1. Location of the experiment in the “Massif des Écrins”, French Alps. Central map presents an aerial picture of the “Pré de Madame Carle” from the Institut Géographique National. Yellow and green flags display the location of stations during the two summers of experiment in 2007 and 2008, respectively. The station name is indicated in the vicinity of each flag. Red circles indicate the two locations of the hydrologic monitoring. The red edge photograph illustrates one of these sites at the outlet of the braided plain (purple area). The yellow edge photographs show two seismic stations. (For interpretation of the references to colour in this figure legend, the reader is referred to the web version of this article.)

1971). The sampling time set to 120 s was sometimes reduced to 60 and 30 s when the discharge was too high to perform a safe measurement. In addition, at each point, we recorded the water level to evaluate the shape of the river section. A complete characterization was carried out in 45–90 min which prevents large variations within the assessed river section. We reproduced such a procedure 1–5 times a day. During phase 2 and in addition to the river section monitoring, we performed a continuous measurement of the water level at a fixed point. The sampling time of less than 15 min during the day provides a well-recorded fluctuation of the water level. However, with the occurrence of a strong rain storm in the night of the 3rd–4th of September, the induced turbulence of the stream destroyed our water gauge height. We replaced it by a second one at the same location but it does not allow us to observe a continuous record of the water level during phase 2. All these hydrological parameters were obtained at the outlet of the braided plain (Fig. 1), upstream of the bridge in order to avoid flow perturbations due to the concrete building. Following Wolman (1954), the grain size distribution of river bed material was also estimated by direct measurements. We collected 1075 samples along 1 m interval profiles for which we measured the minimum, the median and the maximum axis of each sediment particle. We also took advantage of the hourly precipitation rates monitored by Électricité De France (EDF), 6 km south-east of the “Pré de Madame Carle” during both seismic experiments. Finally, the temperature changes were estimated from the temperature sensor that equipped the digital acquisition system of each seismological station. This temperature data can only be interpreted in relative since each acquisition system was installed in a plastic box with a given insolation exposure. By averaging the temperature data at stations, we retrieve an estimate of the temperature variations.

3. Data analyses

3.1. Bed load distribution

The grain size distribution is estimated after sampling a large amount of sediment particles along the river banks (1075

samples). We obtain a minimum, median and maximum D_{90} of 6.2, 9.1 and 12.4 cm, respectively (Fig. 2). Except slight discrepancies for fine grains ($D = 0.2$ – 2 cm), these results are in agreement with the median diameter distribution and the D_{90} of 9 cm estimated by Meunier et al. (2006). The bed load sampled during the two experiments gives a median diameter D_{90} of 0.2 cm and a grain distribution consistent with the one obtained in 2002 ((Meunier et al., 2006), Fig. 2). Despite a time-spacing of 6 years and a different location for the bed load sampling of about 10 m, data collected using Wolman’s method along the river banks and the Helley–Smith sampler for bed load estimate give similar grain size distributions. The bed load distribution exhibits large discrepancies with the distribution in the braided plain. These differences can result from several factors. First, the number of bed load samples is significantly lower than the river bank samples and thus the bed load data might not be representative. Second, the sampled bed load is dependent on the transport capacity of the river. During these experiments, the hydrological conditions may have prevented the

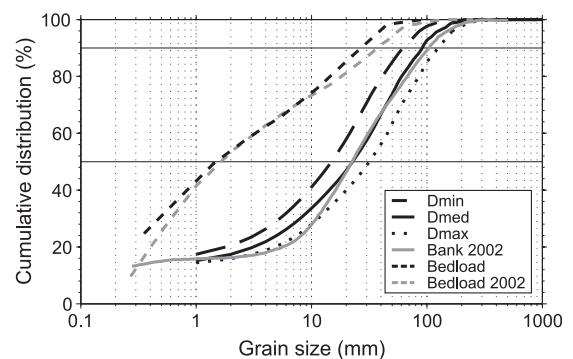


Fig. 2. Grain size distribution of the braided plain computed with 1075 samples collected along the banks and of the bed load material collected over all the study river sections. We present the obtained minimum, median and maximum diameter for the river bank and the bed load size distribution. Results from Meunier et al. (2006) correspond to “Bank 2002” and “Bedload 2002”.

motions of largest particles. More data integrated over space and time might be necessary for both curves to match. Finally, the observed differences could also denote an over-sampling of small grains by the Helley–Smith instrument. Despite these eventual disturbances, the grain size distribution of bed load shows that most of the transported particles are of the order of millimetres. During high water flow the mobilization of a larger grain fraction is suspected, involving particles up to a few tens of centimetres, the typical size of the largest pebbles available along stream. In any case, this transported grain fraction appears to be at least one order of magnitude smaller than along Himalayan rivers, where a D_{90} greater than 60 cm is observed (Mezaki and Yabiku, 1984). Thus, the relevance of a bed load survey with seismic stations installed up to 200 m is risen and the proper conditions of investigation have to be studied.

3.2. Temporal evolution of sediment transport

Following Meunier et al. (2006), we study the evolution of the water discharge and sediment transport rate estimated across some river sections that we assessed during both campaigns. Unsurprisingly our results suggest a relationship between sediment transport rate and water discharge: higher discharges lead to higher sediment transport rate (Fig. 3). This result is consistent with the study of Meunier and colleagues. However, the amplitudes of both water discharge and sediment load are lower in 2007 and 2008 than in 2002. These discrepancies may result from several elements, including the location of the sampling area or the interannual variability of the total water discharge. In July 2002, the sampling area was downstream of the bridge at the output of the braided plain whereas in this study, we sampled the main section of the river located upstream of the bridge (Fig. 1). An alternative explanation can be found in the thermal amplitude of the summer ablation season. Stott and Mount (2007) have shown large differences in water discharges and suspended loads between summers 2003 and 2004, corresponding to exceptionally warm and cold summers, respectively (e.g., Beniston, 2004). In 2003, a water discharge three times higher induces a sediment transport four times larger than in 2004. These results illustrate how the fluctuations of the stream hydrodynamics could influence the sediment transport rate that we collect in the “torrent de St Pierre”.

Furthermore and as previously mentioned (Meunier et al., 2006; Stott and Mount, 2007), our dataset of Julian day 246 supports a good correlation between temperature and water level changes in time (Fig. 4). The water supply appears to follow a trend similar to the temperature variation with a time lag of about 2 h. This time lag is related to the daily melting of snow and ice from the two upstream glaciers. However the next day, this correlation is disrupted with the occurrence of rainfall episodes. Although the increase in water level in the morning coincides with a temperature increase, in the afternoon discharge continues to increase despite a decline in temperature coinciding with the onset of precipitation (Fig. 4). The temperature decrease and its low level in the following days are associated with a dense cloud cover that reduced the duration of insolation and thus the glacier melting. On Julian day 248, a variation of 0.56 m in the water level coincides with some insignificant temperature fluctuation and large precipitation rates (Fig. 4). During these meteorological events, the supply of water to the stream is dominated by rainfalls.

Altogether, the relationships “bed load – water discharge” and “water level – temperature” suggest that temperature can be used as a proxy of the bed load transport during dry weather periods. Since temperature is measured continuously such a relationship will be very useful to interpret seismic noise in terms of river discharge changes.

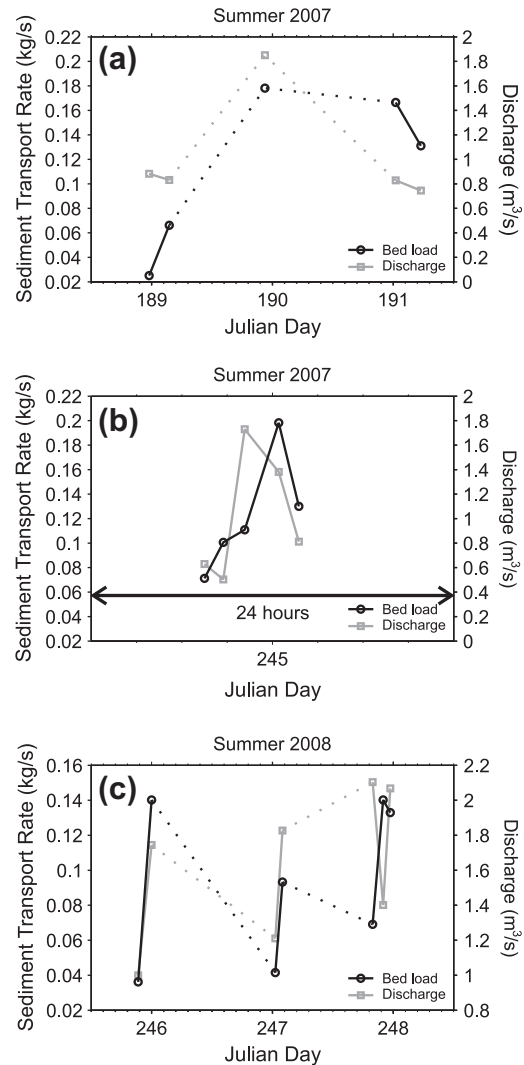


Fig. 3. Compilation of the mean water discharges (grey) and sediment transport rates (black) estimated for the river section studied during the two summers of experiment.

3.3. Spectral analysis of seismic noise

The analysis of the continuous seismic signal consists in calculating the spectral energy radiated in frequency. To do so, we proceed to the computation of the Power Spectral Density (PSD) with a multitaper method (Thomson, 1982; Percival and Walden, 1993). For each station, the continuous signals are cut in windows of 10 min length with 50% of overlap on which we calculate a PSD. Then, we compile the PSD estimates into a spectrogram, as illustrated in Fig. 5. The spectrograms at BOL01, BOL05 and BOL07 (see Fig. 1 for station locations) depict a 24 h fluctuation of the seismic energy in the frequency range 2–40 Hz with a maximum in the afternoon. Some spatial variations are also noticed since the level of seismic noise is larger at BOL05 and BOL07 than BOL01 which is located at the outlet of the braided plain. Superimposed on the daily cyclicity, we notice a trend in the signal with longer periods of 5–10 days, especially between 40 and 60 Hz at BOL05 and BOL07. These long period trends are interrupted by strong bursts of high-frequency seismic noise that are well revealed at BOL07. These sudden increases of seismic noise are spread over the entire 2–90 Hz frequency band (Fig. 5c). At BOL05, these bursts of seismic energy are seen but the extension to very high frequencies (>60 Hz) is missing (Fig. 5b).

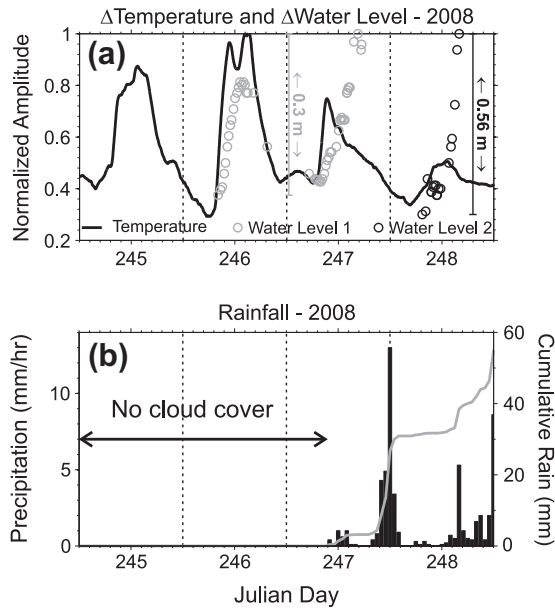


Fig. 4. (a) Comparison of the temperature variation (black) with the measured water level in cm (circle) during the second experiment. Water "Level 1" and "Level 2" stand for the data measured with the first and the second water gauge height, respectively. (b) Precipitation rate (mm/h) measured at the EDF station of "Pelvoux–Les Claux", 6 km south-east of the "Pré de Madame Carle" (black bars) and the cumulative rain in mm (grey line) during phase 2.

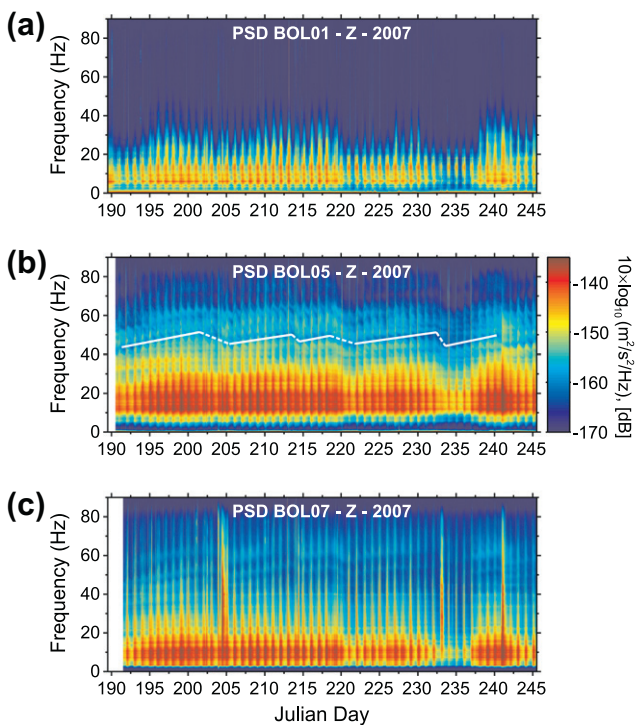


Fig. 5. Spectrograms of vertical seismograms at BOL01 (a), BOL05 (b) and BOL07 (c). The seismic energy is given in decibel (dB) in relative to the velocity. Red and blue colours stand for high and low amplitudes, respectively. A similar scale is used for all the spectrograms. Note the daily periodicity of the spectral activity and the appearance of a longer period signal (highlighted with white lines on BOL05) between 40 and 60 Hz at BOL05 and BOL07. These long period signals are cut by transient events of high-frequency seismic noise. (For interpretation of the references to colour in this figure legend, the reader is referred to the web version of this article.)

In the case of BOL02, the 24 h periodicity shows a different behaviour which may be linked to human activity since the station is located close to the road (Fig. 6). We illustrate this discrepancy in a daily spectrogram averaged over a period of 7 days where no rainfall is reported (from Julian day 207 to 213; Fig. 7d). By excluding days with precipitation, we simplify the number of contributors for the seismic noise generation. We limit here the water supply of the "torrent de St Pierre" to the melting of glaciers. The comparison between BOL02 and BOL05 signals reveals: (1) a time delay of about 4 h for the increase of high-frequency seismic energy at BOL05, (2) a similar time at 3 p.m. (U.T.) for the maximum of energy and (3) a more persistent band of excited frequencies (10–30 Hz) at BOL05 than at BOL02. The mean noise level in a 2–60 Hz frequency band for both daily spectrograms highlights these observations (Fig. 6c). The energy variation at BOL05 and the temperature changes follow a similar pattern for the same period of time. In contrast, at BOL02 the variation of the seismic noise level exhibits a shape close to a step function with a maximum during the day which is typical of human-made seismic noise (McNamara and Buland, 2004). Another discriminator is the time-signature of the contributor to high-frequency seismic noise. At BOL02, it is induced by discontinuous, short (~ 20 s) and high-amplitude signals generated by traffic on the road while the signal at BOL05 is continuous and homogeneous in amplitude. Together these observations are useful to discriminate between human and natural sources in the high-frequency seismic noise and support that except BOL02, all stations are actually not disturbed by anthropogenic activities.

To assess the river effect in the natural sources of noise, we analyze the temporal variations of the mean seismic energy recorded at BOL01, BOL05 and BOL07 in the 2–60 Hz frequency band (Fig. 7). These fluctuations are compared with the temperature variation for the same period of time. First, the daily and the long period evolution of about 10 days of the seismic energy are coherent from one station to another (Fig. 7). Besides, the comparison with the temperature variation reveals a good agreement for both time scales. Thus during summer 2007, peaks of temperature are associated with large seismic energies and the lowest high-frequency noise happens for cold days (Fig. 7). These observations suggest a strong link between the recorded seismic noise and the hydrology of the stream for which the water supply is mainly controlled by melting. Nevertheless for some days (grey shaded areas in Fig. 7), we record larger amplitudes of seismic noise than if temperature was the only key parameter of the stream hydrology. These anomalies of seismic energy actually occur while bursts of seismic noise are well detected at BOL07. These transient events always happen for days with a weak diurnal thermal fluctuation. The comparison with precipitation rates indicates that these particularly "noisy" days are generated by large rainfall events. The cloud cover reduces the daily thermal amplitudes and the melting of glaciers. However, the amount of water brought by rains may fill and exceed the lack of water from melting since the highest peaks of seismic noise are during rainy days at BOL07 (Fig. 7). Finally, the relative amplitudes of these peaks, over the entire time-series, are larger at BOL07 than at BOL05 and than at BOL01. This spatial pattern suggests a dominant effect of these transient events with an increasing distance from the outlet of the braided plain.

During phase 2, both dry and wet climatic conditions are encountered. On one hand, during Julian days 245 and 246 the melting of glaciers is the only source of water (Fig. 4b). On the other hand, over Julian days 247 and 248 strong rainfalls occur with a peak rate of 13 mm/h and a total cumulative rain of almost 60 mm, when only 80 mm were recorded during the two months of phase 1 (Fig. 7d). The spectrograms calculated at ECR01, ECR03 and ECR04 display spectral features and temporal evolution of the seismic noise like we had observed one year before (Fig. 8).

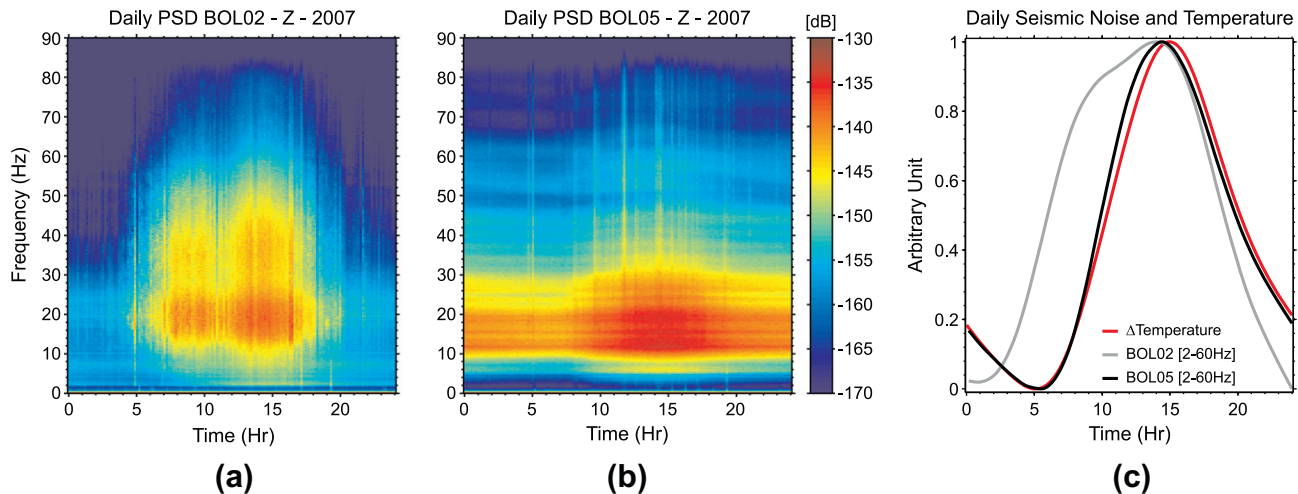


Fig. 6. Mean daily spectrograms computed over a period of 7 dry days (Julian day 207–213) at BOL02 (a) and BOL05 (b). The seismic energy is given in decibel (dB) in relative to the velocity. Red and blue colours stand for high and low amplitudes, respectively. A similar scale is used for both spectrograms. (c) Mean daily variation of the temperature (red) and mean seismic noise level in the 2–60 Hz frequency band at BOL02 (grey) and BOL05 (black) for the same period of time. (For interpretation of the references to colour in this figure legend, the reader is referred to the web version of this article.)

As expected during the two first days of recordings, the spectral activity shows a daily fluctuation consistent with temperature and water level changes. In addition one can note a systematic decay of the energy and a shift of the maximum energy towards lower frequencies with the distance from the stream (see Fig. 1 for station locations). Such a pattern may reflect the strong attenuation of the highest frequencies of the seismic waves propagating in the unconsolidated sediments that compose the braided plain. Another feature is the occurrence of a more persistent frequency band at 2–10 Hz. This dominant frequency band was also noticed at phase 1 stations like BOL01, BOL05 and BOL07 (Fig. 5).

During the last two days of phase 2, intense rainfalls affect the daily fluctuation of the seismic energy. The spectral energy is distributed over a broad range of frequencies. The highest seismic noise levels are no longer coherent with the temperature variations (Figs. 4a and 8) but are still consistent with the water level changes (Fig. 9). The highest water fluctuations on Julian day 248 correspond with the largest seismic energy recorded at stations. Moreover for the largest rain episode (Julian day 247–248), one can notice at ECR04 a high level of seismic noise in the 60–90 Hz frequency band. It may indicate a different source origin for this specific high-frequency noise. This one could be induced by the rain falling on rock debris that are more distributed close to the steep slopes surrounding the braided plain.

Therefore, the data collected during summers 2007 and 2008 suggest that the river hydrology mainly controls the variations of seismic noise level. In the following section, we will discuss in details the relationship between the measured seismic noise and the hydrodynamic parameters of the “torrent de St Pierre”.

4. Seismic monitoring of hydrology and sediment transport

4.1. Water level – seismic noise relationship

As detailed in the previous section, the daily variation of the seismic noise is coherent with the diurnal increase of both water discharge and sediment transport (Meunier et al., 2006; Stott and Mount, 2007). Furthermore, we have also mentioned specific spectral energy contents for some stations, like the sudden bursts of high-frequency seismic noise observed at BOL07, ECR01, ECR03 and ECR04 during rainstorms (Figs. 5c and 8). We suspect that these seismic noise features are generated by the joint effect of

flowing water and bed load motions. To test this hypothesis, we carefully compare seismic observations with hydrological measurements. Here, we take advantage of the high sampling rate hydrological data, collected during phase 2, to perform a detailed comparison with the continuous seismic signals showing time and spectral content variations. We proceed to the calculation of the mean noise level around a given frequency f_0 and for a restricted band-width of 1 Hz. Using a least square minimization, we then determine the best linear relationship between the measured water level and the estimated seismic energy. The misfit in frequency of this hydrologic–seismic relationship is presented on Fig. 10.

The error distribution in the high-frequency band (>1 Hz) gives a similar pattern for all stations. We obtained a better fit for decreasing frequencies. From this error analysis and assuming that a linear relation exists between water level and seismic noise, it appears that the 3–9 Hz frequency band is best related to the water level (Fig. 11). The three stations give a similar result, especially for seismic noise amplitude lower than –126 (at ECR01) and –128 dB (at both ECR03 and ECR04) where the slope of this linear regression is equivalent. Since we observe a good agreement between these data, and because both water gauge heights were installed on the same exact location where only the base level had changed, we can assume that a similar seismic energy should refer to an equivalent water level. This assumption allows us to reconstruct a continuous water level time-series using 12 tie points within the seismic noise range of –130 and –127 dB (Fig. 11). Above the seismic noise values of –126 dB for ECR01 and –128 dB for ECR03 and ECR04, the statistical relationships between noise and water level exhibit a threshold. This feature may be related to the classical concept of critical shear stress used to describe the river transport capacity (e.g., du Boys, 1879; Shields, 1936). If the stress of the flowing water on a stream bed is less than a critical shear stress, particles within the river will remain motionless. Movements will be observed only if the stress exerted by the flowing water exceeds this critical shear stress. The fluvial shear stress τ exerted by the flowing water is defined as

$$\tau = \rho gSR, \quad (1)$$

where ρ is the fluid density, g is the gravity, S is the water surface slope, and R is the hydraulic radius, the ratio of the area of section flow to the wetted perimeter. Assuming a cross-sectional profile of

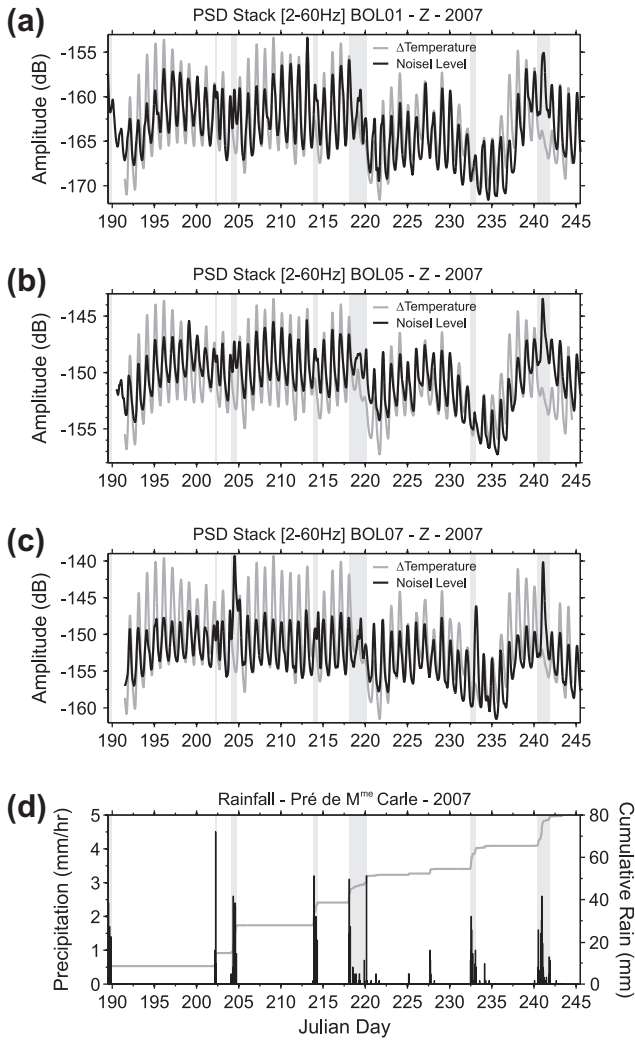


Fig. 7. Mean seismic noise level in the 2–60 Hz frequency band (black) at BOL01 (a), BOL05 (b) and BOL07 (c). The temperature variation for the same period is also indicated in grey. (d) Precipitation rate (mm/h) measured at the EDF station of “Pelvoux–Les Claux”, 6 km south-east of the “Pré de Madame Carle” (black bars) and the cumulative rain in mm (grey line) during the same period. On each figure, a grey area marks a strong episode of rain.

a typical braid with a channel bounded by wide and nearly flat bars (Fig. 12a), R increases with water level until a critical value H_c associated with the flattening of the stream profile (Fig. 12b). This suggests that the observed threshold in seismic noise energy in the frequency band 3–9 Hz can be related to the geometry of the braided river itself which leads to a reduction in the basal shear stress during channel overflow.

4.2. Sediment transport – seismic noise relationship

The previous result reveals that the measured water level is poorly related to the seismic energy estimated for frequencies above 40 Hz. At these frequencies the seismic noise may be induced by other contributors like the sediment transport. To test this eventuality, following a similar approach as the one described in Section 4.1, we try to link the seismic energy with the bed load measurements through a linear relationship. For this purpose, we use the data collected along the seven river cross-sectional profiles acquired during phase 2 (Fig. 3c). The result of this analysis reveals a complex pattern of the error distribution at all stations (Fig. 13). Nevertheless at low frequencies a unique pattern is observed and

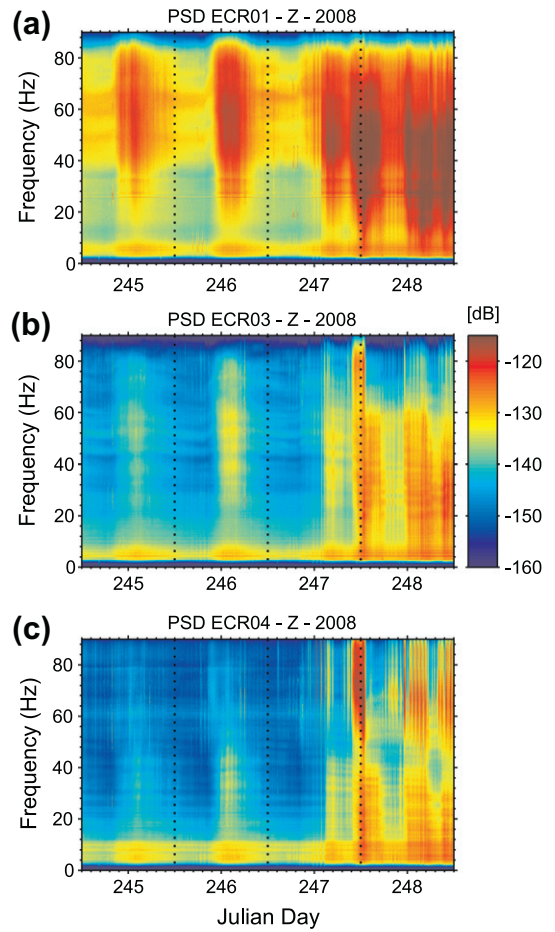


Fig. 8. Spectrograms of vertical seismograms at ECR01 (a), ECR03 (b) and ECR04 (c). The seismic energy is given in decibel (dB) in relative to the velocity. Red and blue colours stand for high and low amplitudes, respectively. A similar scale is used for all the spectrograms. (For interpretation of the references to colour in this figure legend, the reader is referred to the web version of this article.)

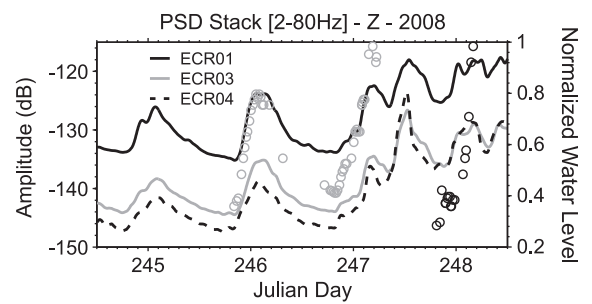


Fig. 9. Mean seismic noise level in the frequency band 2–80 Hz for the phase 2 at ECR01 (black), ECR03 (grey) and ECR04 (black dash). We also report on this figure both water level variations which are normalised to their maximum amplitude (Fig. 4).

displays a decrease of the misfit function from 15 to 40 Hz. Above 40 Hz only ECR01, the closest station to the stream, exhibits a similar decrease of the error with an increasing frequency. These complex relationships underline our difficulties to define the most appropriate frequency band for a seismic monitoring of bed load. However, at ECR01 the frequencies that best explain the bed load measurements are the ones that most poorly describe the seismic noise of the water. In addition, the specific location of ECR01 (only 15 m away from the main channel) may play a dominant role in

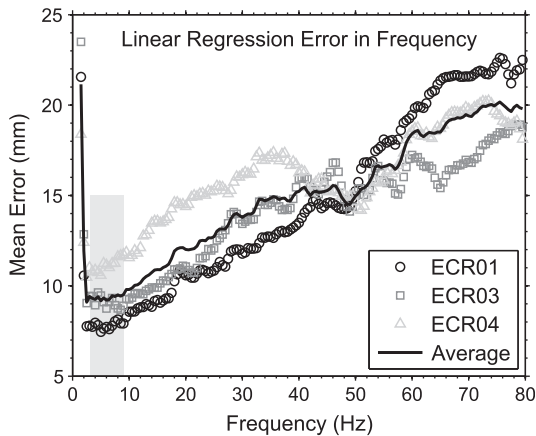


Fig. 10. Misfit function in frequency for the linear regression of a relationship between seismic noise and water level at ECR01 (black circle), ECR03 (grey square) and ECR04 (grey triangle). The black line corresponds to the mean misfit function at these three stations. The grey shaded area represents the best frequency band to express this linear relationship.

these observations. The impossibility to define a well constrained linear relationship between sediment load and seismic noise may have multiple origins. (1) Such a relationship could actually be non-linear. (2) The available bed load estimates are not sufficient. (3) The spatial variability of the sediment transport rate affects the seismic monitoring at the scale of the braided plain. During phase 2, the seismic stations and the bed load sampling site were obtained more than 500 m apart (Fig. 1). Thus, our bed load dataset might not be representative of the sediment transport over the “Pré de Madame Carle”. (4) There is no unique frequency band that describes the bed load transport. Some or all of these points prevent us from defining a proper relationship.

Following Eq. (1), the expression of the fluvial shear stress τ has a linear dependency on the hydraulic radius R . Since we notice a similar evolution of the water level with both the seismic noise level at 3–9 Hz and the hydraulic radius, we assume that the seismic energy in this frequency band is a proxy of τ . With such a proxy, we can compare this continuous monitoring of the stream hydrology with the seismic energy recorded at higher frequency bands to explore some potential observation of bed load transport. Fig. 14a shows the variation of the seismic noise level recorded at ECR01 for three frequency bands as a function of the assumed fluvial shear stress. The selected bands sample low (9–15 Hz), intermediate (21–27 Hz) and high (45–51 Hz) frequencies. Since our proxy of the fluvial shear stress imposes a linear relationship for the fluctuation of seismic noise at 3–9 Hz, we introduce a bias in the study of the variation of the seismic energy. To discard this artefact, we remove the observed linear trend that is the seismic energy at 3–9 Hz from each frequency band. After this correction, the variation of the seismic energy in the 3–9 Hz band is equal to zero with an increase of τ . Thus, in the following, we only look for variations of seismic noise related to changes in our proxy of the fluvial shear stress. For low shear stress and for all frequency bands, an increase of τ implies no significant variation of seismic noise (Fig. 14a). In contrast for higher shear stress our results reveal a threshold behaviour, which depends on the assumed frequency band: higher is the frequency band, lower is the critical shear stress.

Based on a natural experiment in a river channel, Huang et al. (2007) have shown a frequency signature of the ground vibrations produced by single particle impacts with the grain size. The authors observed that the motions of large particles generate a peak of energy at lower frequencies than for smaller grains. The evolution pattern we notice in the activation of lower frequencies

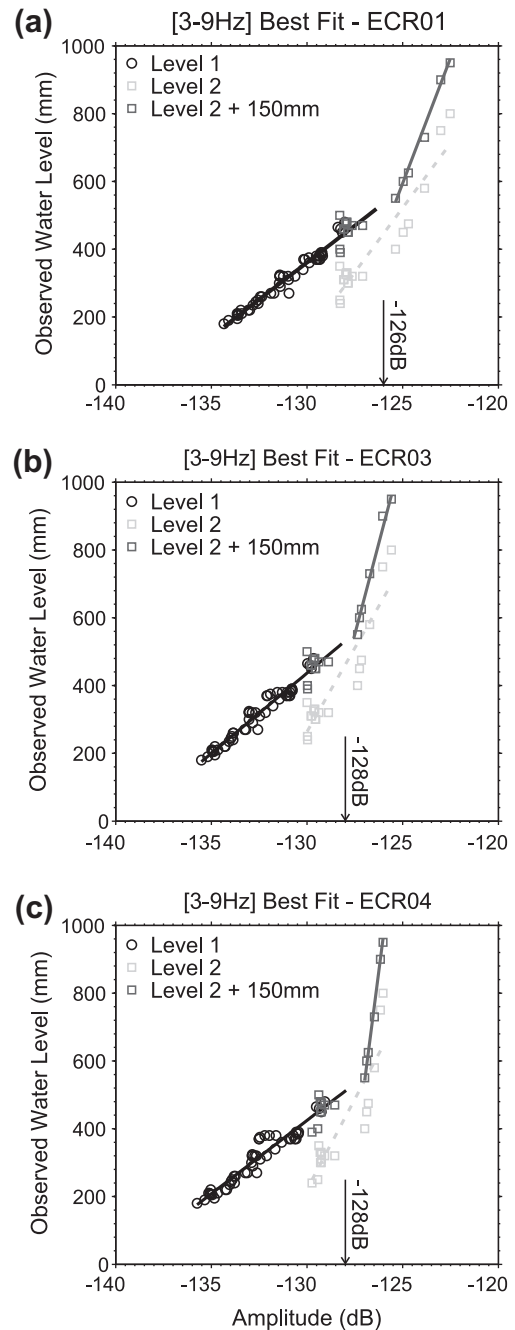


Fig. 11. Best fits for the linear relationship of the seismic noise in the 3–9 Hz frequency band and the water level for gauge 1 (black) and for gauge 2 (dash line) at ECR01 (a), ECR03 (b) and ECR04 (c). The retained frequencies are previously determined from the error analysis (Fig. 10).

with an increased τ confirms their results. The variations of seismic energy in this selected frequency band exhibit a second interesting feature. In the 45–51 Hz frequency band, with a continuous increase of the fluvial shear stress and the overpass of a second threshold τ_{cSat} , we notice a constant seismic noise level (Fig. 14a). Meanwhile, none of the two lower frequency bands (9–15 Hz and 21–27 Hz) describes this feature. Since the frequency content may reflect the size of particles that are mobilized, such an amplitude threshold could indicate the influence of a transport capacity. Indeed, all the particles that affect the 41–45 Hz frequency band are probably already in motion and a continuous increase of τ does not affect these grain sizes anymore.

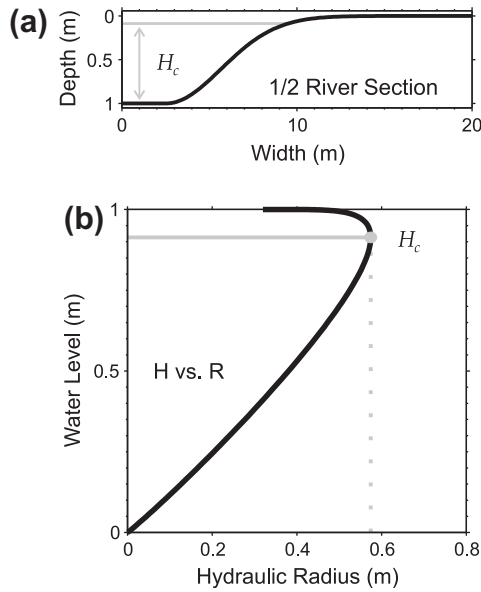


Fig. 12. (a) Cross-sectional river profile of a typical braid with a channel bounded by wide and nearly flat bars. (b) Variation of the hydraulic radius R with the water level H associated with the profile displays in (a). H_c is the critical water level.

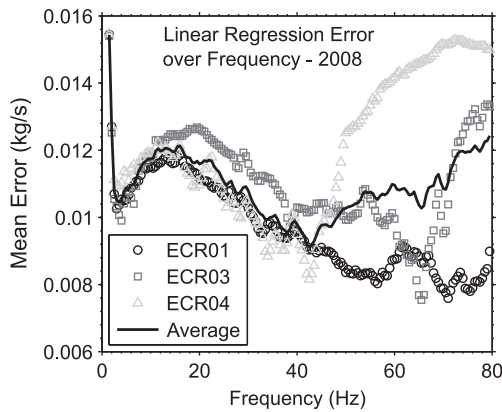


Fig. 13. Misfit function in frequency for the linear regression of a relationship between seismic noise and sediment transport rates at ECR01 (black circle), ECR03 (grey square) and ECR04 (grey triangle). The black line corresponds to the mean misfit function at these three stations. Note that only ECR01 shows a constant trend with lower error values for higher frequencies.

Furthermore, the hydrological conditions are not efficient to mobilize a wide range of particle sizes since the lowest frequency bands are not affected by such a saturation threshold (Fig. 14a).

In addition to these observations, the spectrograms of the seismic recordings during a flood episode also reveal a frequency content that varies with the hydrological conditions. During the night of Julian day 247–248 (Fig. 14b), with the occurrence of a large rainstorm (Fig. 4b), we initially record a seismic energy at high frequencies that shifts to lower ones following an increase of the water discharge. As a consequence, a constant level of seismic energy displays some delay to activate low frequencies (Fig. 14b). Afterwards with the ending of precipitation, we notice the extinction of the lowest frequencies before the highest ones while water discharge decreases. These observations suggest again a link between the frequency content and the transport capacity of the river.

Some interpretations clearly depend on the assumption of our proxy of the fluvial shear stress. Unfortunately, the amount of

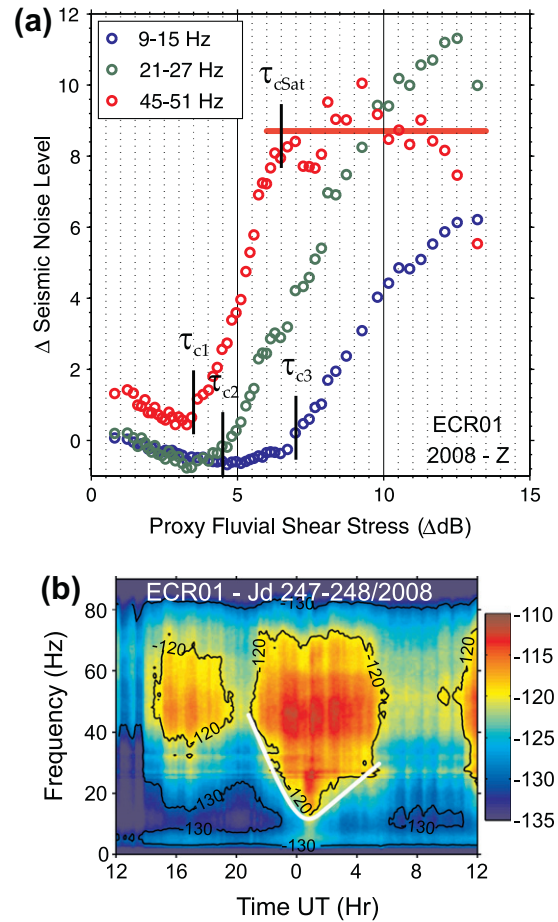


Fig. 14. (a) Variations of the seismic energy in the 9–15 Hz (blue), 21–27 Hz (green) and 45–51 Hz (red) frequency bands as a function of a proxy of the fluvial shear stress. The linear trend induced by the seismic energy at 3–9 Hz is removed from the bands displayed, according to the methodology described in the text. As a consequence, both axes refer to a variation of seismic noise given in dB. Note the progressive activation of lower frequency bands with an increasing fluvial shear stress ($\tau_{c1} < \tau_{c2} < \tau_{c3}$). τ_{cSat} represents a threshold beyond which the 45–51 Hz seismic energy remains constant despite an increasing fluvial shear stress. (b) Contour levels of the seismic energy recorded at ECR01 in the night of Julian day 247–248. White line highlights the spectral pattern that we discuss in Section 4.2 and that suggests the influence of bed load transport. (For interpretation of the references to colour in this figure legend, the reader is referred to the web version of this article.)

bed load data collected during the experiment is not sufficient to support such a hypothesis. Besides, the saturation of seismic noise level in the 3–9 Hz frequency band with the increased water level could have other explanations, like the different site locations of the water gauge height and the seismic stations. The water level data documents the water discharge of a unique channel at the output of the “Pré de Madame Carle”. However in the braided plain where seismometers are located, the increase of water level could reveal some overflow in secondary distant channels. The threshold of seismic energy could represent an altered sensitivity to record the seismic signal from flowing water and sediment transport in these secondary channels. Nevertheless in regards to our field experience, this latter explanation should only affect a minor part of the recorded seismic energy. During our two seismic experiments the main channel of the braided plain was clearly dominant for the development of hydrologic and geomorphic processes. In addition for the lowest frequency bands (<30 Hz), the spectral pattern induced from the relationship of the seismic noise with our proxy of fluvial shear stress is also noticed at stations ECR03 and

- Burtin, A., Vergne, J., Rivera, L., Dubernet, P.-P., 2010. Location of river induced seismic signal from noise correlation functions. *Geophys. J. Int.* 182 (3), 1161–1173.
- du Boys, M.P., 1879. Étude du régime du Rhône et de l'action exercée par les eaux sur un lit à fond de graviers indéfiniment affouillable. vol. 18 of 5. *Annales des Ponts et Chaussées*.
- Eugene, F., 1951. Measurement of bed-load sediment. *Trans. Am. Geophys. Union* 32, 123–126.
- Froehlich, W., 2003. Monitoring bed load transport using acoustic and magnetic devices. In: Bogen, J., Fergus, T., Walling, D.E. (Eds.), *Erosion and Sediment Transport Measurement in Rivers, Technological and Methodological Advances*. AHS Publication No. 283, Wallingford, pp. 201–210.
- Galy, A., France-Lanord, C., 2001. Higher erosion rates in the Himalaya: geochemical constraints on riverine fluxes. *Geology* 29, 23–26.
- Govi, M., Maraga, F., Moia, F., 1993. Seismic detectors for continuous bed load monitoring in a gravel stream. *Hydrol. Sci.* 38 (2), 123–132.
- Helley, E., Smith, W., 1971. Development and Calibration of a Pressure-Difference Bedload Sampler. US Geological Survey Open-File Report 18.
- Huang, C.-J., Yin, H.-Y., Chen, C.-Y., Yeh, C.-H., Wang, C.-L., 2007. Ground vibrations produced by rock motions and debris flows. *J. Geophys. Res.* 112. doi:10.1029/2005JF000437.
- Johnson, P., Muir, T., 1969. Acoustic detection of sediment movement. *J. Hydraulic Res.* 7, 519–540.
- Lane, E., Borland, W., 1951. Estimating bed load. *Trans. Am. Geophys. Union* 32, 121123.
- Lavé, J., Avouac, J.-P., 2001. Fluvial incision and tectonic uplift across the Himalayas of central Nepal. *J. Geophys. Res.* 106 (B11), 26,561–26,592.
- Leopold, L.B., Emmett, W.W., 1976. Bedload measurements, East Fork River, Wyoming. *Proc. Natl. Acad. Sci. USA* 73 (4), 1000–1004. <http://www.pnas.org/content/73/4/1000.abstract>.
- McNamara, D.E., Buland, R.P., 2004. Ambient noise levels in the continental United States. *Bull. Seism. Soc. Am.* 94 (4), 1517–1527.
- Meunier, P., Métivier, F., Lajeunesse, E., Mériaux, A.S., Faure, J., 2006. Flow pattern and sediment transport in a braided river: the “torrent de St Pierre” (French Alps). *J. Hydrol.* 330, 496–505.
- Mezaki, S., Yabiku, M., 1984. Channel morphology of the Kali Gandaki and the Narayani rivers in central Nepal. *J. Nepal Geol. Soc.* 4, 161–176.
- Percival, D.B., Walden, A.T., 1993. *Spectral Analysis for Physical Applications: Multitaper and Conventional Univariate Techniques*. Cambridge University Press.
- Pratt-Sitaula, B., Garde, M., Burbank, D.W., Oskin, M., Heimsath, A., Gabet, E., 2007. Bedload-to-suspended load ratio and rapid bedrock incision from Himalayan landslide-dam lake record. *Quaternary Res.* 68 (1), 111–120.
- Rickenmann, D., McArdell, B.W., 2007. Continuous measurement of sediment transport in the Erlenbach stream using piezoelectric bedload impact sensors. *Earth Surf. Process. Land.* 32 (9), 1362–1378.
- Rickenmann, D., McArdell, B.W., 2008. Calibration of piezoelectric bedload impact sensors in the Pitzbach mountain stream. *Geodin. Acta* 21 (1–2), 35–52.
- Schumm, S., 1986. *Studies in Geophysics: Active Tectonics*. Washington, DC, National Academy Press, pp. 80–94. (Chapter Alluvial river response to active tectonics).
- Shields, A., 1936. *Anwendung der Aehnlichkeitsmechanik und der Turbulenzforschung auf die Geschiebebewegung*. Mitt. Preuss. Versuchsanst. Wasserbau Schiffbau 26, pp. 26. (English translation by W.P. Ott and J.C. van Uchelen, 36 pp., US Dep. Agric. Soil Conser. Serv. Coop. Lab., Calif., Inst. Technol., Pasadena, 1936.).
- Sklar, L., Dietrich, W.E., 1998. *Rivers Over Rock: Fluvial Processes in Bedrock Channels* (Vol. Monograph 107), Washington, DC, American Geophysical Union, pp. 237–260. (Ch. River longitudinal profiles and bedrock incision models: stream power and the influence of sediment supply).
- Sklar, L.S., Dietrich, W.E., 2001. Sediment and rock strength controls on river incision into bedrock. *Geology* 29 (12), 1087–1090.
- Stott, T., Mount, N., 2007. Alpine proglacial suspended sediment dynamics in warm and cool ablation seasons: implications for global warming. *J. Hydrol.* 332, 259–270.
- Thomson, D.J., 1982. Spectrum estimation and harmonic analysis. *Proc. IEEE* 70 (9), 1055–1096.
- Thorne, P., 1986. The acoustic measurement of gravel transport. In: *Proceedings of the Fifth International Conference on Electronics for Ocean Technology*, Edinburgh, 24–26 March, 1987. No. 72. Institution of Electronic and Radio Engineers, London, pp. 63–70.
- Thorne, P., Hanes, D., 2002. A review of acoustic measurements of small-scale sediment processes. *Cont. Shelf Res.* 22, 603–632.
- Tucker, G.E., Whipple, K.X., 2002. Topographic outcomes predicted by stream erosion models: sensitivity analysis and intermodel comparison. *J. Geophys. Res.* 107. doi:10.1029/2001JB000162.
- Turowski, J.M., Lague, D., Hovius, N., 2007. Cover effect in bedrock abrasion: a new derivation and its implications for the modeling of bedrock channel morphology. *J. Geophys. Res.* 112. doi:10.1029/2006JF000697.
- van den Berg, J.H., 1995. Prediction of alluvial channel pattern of perennial rivers. *Geomorphology* 12 (4), 259–279.
- Wolman, M., 1954. A method of sampling coarse river-bed material. *Trans. Am. Geophys. Union. Hydraul. Res. Stn.* 35, 951–956.